

A hybrid model for chaotic front dynamics: From semiconductors to water tanks

A. Amann,¹ K. Peters,² U. Parlitz,² A. Wacker,¹ and E. Schöll¹

¹*Institut für Theoretische Physik, Technische Universität Berlin, Hardenbergstraße 36, 10623 Berlin, Germany*

²*Drittes Physikalisches Institut, Universität Göttingen, Bürgerstraße 42-44, 37073 Göttingen, Germany*

(Dated: July 2, 2003)

We present a general method for studying front propagation in nonlinear systems with a global constraint in the language of hybrid tank models. The method is illustrated in the case of semiconductor superlattices, where the dynamics of the electron accumulation and depletion fronts shows complex spatio-temporal patterns, including chaos. We show that this behavior may be elegantly explained by a tank model, for which analytical results on the emergence of chaos are available. In particular, for the case of three tanks the bifurcation scenario is characterized by a modified version of the one-dimensional iterated tent-map.

PACS numbers: 05.45.-a, 05.45.Ac, 72.20.Ht, 73.21.Cd,

Keywords: front models, tank models, hybrid models, iterated maps

Introduction. Moving fronts are the source of complex patterns in very different areas of physics [1], chemistry [2, 3] and even biology [4, 5]. While the propagation of single fronts is well understood for many systems, only little is known on how front generation and annihilation processes or collisions between fronts influence the possible bifurcation scenarios.

For the sake of concreteness we illustrate our method with a semiconductor superlattice system, which is well studied experimentally and theoretically [6, 7, 8, 9, 10, 11] and shows a wide range of complex front patterns (cf. Fig. 1) including chaos [12, 13, 14]. Similar front patterns occur in many other systems [15], e.g., spatially continuous semiconductor models describing impurity impact ionization breakdown [16] or globally coupled heterogeneous catalytic reactions [17]. Our aim is to point out a striking connection of those front patterns with discrete hybrid models of n tanks such as they occur, for instance, in industrial production processes [18], and derive a simple description of the front generation and annihilation dynamics in terms of an n -tank model which allows for an analytical treatment of the bifurcation scenarios. In particular, an unusual chaotic scenario will be characterized by this generic model. We stress that the presented methods do not depend on the peculiarities of the superlattice model, and are expected to be equally applicable to other front systems with global coupling.

In order to formulate a generic model for front propagation, we will first develop a *front model* based on the spatio-temporal dynamics in a semiconductor superlattice. The dynamical variables are the positions of the accumulation and depletion fronts which evolve with a velocity determined by the number of fronts present in the system. The number of fronts changes according to simple rules which mimic generation of fronts at the emitter and the annihilation of fronts. Such models are quite general and similar ideas have been sketched for front propagation in bulk GaAs [16]. It will be shown that this front model is identical to an n -tank *switched arrival system* [18, 19], if one identifies the spacing x_i (see Fig. 1) between the leading depletion and the trailing accumulation front with the filling heights of the tanks.

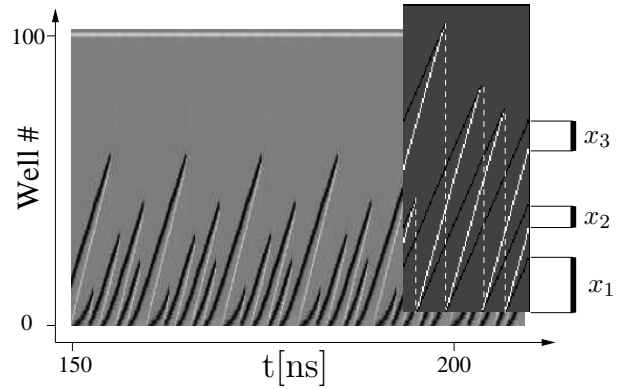


FIG. 1: (a) Space-time plot of the electron density evolution in a semiconductor superlattice. Electron accumulation and depletion fronts are indicated by light and dark shading, respectively. The full microscopic sequential tunneling model of Ref. 14 for $N=100$ quantum wells and contact conductivity $\sigma = 0.5 \text{ } \Omega^{-1}m^{-1}$ is used for a bias $U = 0.95 \text{ V}$. The inset shows a simplified view of the pattern, which is adopted in the front and the tank model. The dashed lines denote the switching times t_m .

The tanks drain at a constant rate μ , while one of the tanks is connected to a server and filled at a rate $\lambda = \tilde{n}\mu$ (Fig 2), where \tilde{n} is the number of tanks which are not empty. In the present model the server will switch to a different tank, if this tank is empty and the filling level of the currently filled tank is larger than x_{min} . In the simplest case $n = 3$, the tank-model transforms into a one-dimensional iterated map which is very similar to the well known tent-map. We will show that the front dynamics in semiconductor superlattices as simulated in [14] can largely be explained by such a one-dimensional map. In particular, atypical border collision bifurcations occur [20]. The general type of models we consider here is called *hybrid* since they contain continuous as well as discrete state variables.

Modeling the front dynamics. The superlattice dynamics is described by the electron densities $n_m(t)$ in the quantum wells, labeled by $m = 1, 2 \dots N$. The current

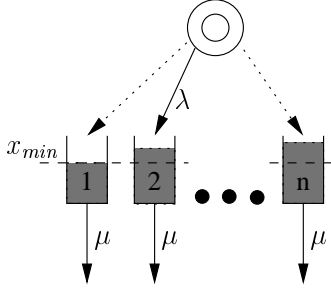


FIG. 2: Scheme of an n -tank switched arrival system with minimal filling height x_{min} .

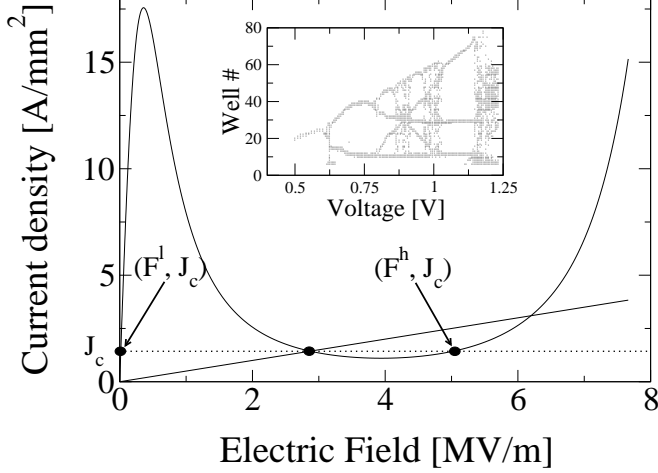


FIG. 3: Current density vs electric field characteristic at the emitter barrier (straight line, Ohmic conductivity $\sigma = 0.5 \text{ } \Omega^{-1}\text{m}^{-1}$) and between two neutral wells (N-shaped curve) for the microscopic superlattice model [14]. J_c denotes the intersection point of the two characteristics. F^l and F^h are the stable low and high field states, respectively, for the current density J_c . Inset: Positions where accumulation and depletion fronts annihilate vs. voltage.

density $J_{m \rightarrow m+1}(n_m, n_{m+1}, F_m)$ between adjacent wells is evaluated by the sequential tunneling model, where $F_m < 0$ is the electric field between these two wells [10]. A microscopic calculation of $J_{m \rightarrow m+1}$ yields an N-shaped current density vs. electric field characteristic as depicted in Fig. 3. In the electrically neutral regions of the superlattice, there are two stable states for fixed current density J , one at a low field $F^l(J)$ and one at a high field $F^h(J)$ (Fig 3). Since in the following J is varied only in a small range, we make the approximation that both fields do not depend on the current density, and set $F^l(J) = 0$, $F^h(J) = F^h > 0$.

The emitter boundary condition (at well $m = 1$) is characterized by its intersection point J_c with the characteristics between neutral wells. For small J_c propagating inhomogeneous field distributions alternating between F^l and F^h occur, see Fig. (1). For a transition from a *low field domain* $F_m = 0$ to a *high field domain* $F_n = -F^h$ ($n > m$) a negatively charged electron accumulation front

located at the domain boundary, is required by Poisson's equation. Let us denote by a_i the distance of its center of charge from the emitter. The index $i = 1 \dots N_a$ labels different accumulation fronts such that $a_i < a_{i+1}$, where N_a is the total number of accumulation fronts in the system. Similarly, a transition from a high field domain to a low field domain can be attributed to an electron depletion front whose center of charge is located at d_i with $i = 1 \dots N_d$, and N_d the number of depletion fronts. Since we only allow for alternating accumulation and depletion fronts, we have $N_d - N_a \in \{-1, 0, 1\}$.

The applied voltage U between emitter and collector defines the partial length $L_h = U/F^h$ of the superlattice which is at high field. This imposes a global constraint on the front positions by

$$L_h = \sum_{i=1}^{N_d} d_i - \sum_{i=1}^{N_a} a_i \mod L. \quad (1)$$

Here L denotes the total length of the superlattice. The expression $\mod L$ in (1) means that L has to be added if $a_{N_a} > d_{N_d}$ such that $L_h \in [0, L]$.

The front velocities are given functions of the total current $\dot{a}_i = v_a(J)$, $\dot{d}_i = v_d(J)$, as shown in Refs. [21, 22]. Differentiating eq. (1) yields $v_d(J)/v_a(J) = N_a/N_d$. This determines the current $J(N_a/N_d)$, which is a monotonically increasing function, as $v_d(J)$ and $v_a(J)$ are increasing and decreasing, respectively [14]. Rescaling the time such that $v_a + v_d = 2$ gives

$$v_a = \frac{2N_d}{N_a + N_d} \quad v_d = \frac{2N_a}{N_a + N_d} \quad (2)$$

Front injection at the emitter is governed by J_c . For $J < J_c$ the region close to the emitter is pinned at a low field [10]. Hence an accumulation front is injected, if the preceding front is a depletion front. Due to the finite width and buildup time of the fronts new fronts can not be injected arbitrarily fast. Phenomenologically we therefore introduce a distance parameter p_h , and assume that front generation is suppressed while $d_1 < p_h$, where d_1 is the position of the first depletion front. In the same fashion, a depletion front is injected if J rises above J_c and $p_l < a_1$, where p_l is a parameter describing the minimum front distance for depletion front injection. As the current J is a monotonic function of N_a/N_d , the condition $J \geq J_c$ can be transformed into $N_a/N_d \geq r_c$ with a new critical parameter r_c .

The processes which reduce the number of fronts are collisions of two fronts of opposite polarity and the running out of fronts at the collector. Both processes affect N_a/N_d and potentially trigger generation of a new front at the emitter.

Let us summarize the rules for front dynamics:

FI The positions of the accumulation fronts a_i for $i = 1 \dots N_a$ and depletion fronts d_i for $i = 1 \dots N_d$ evolve according to $\dot{a}_i = v_a$ and $\dot{d}_i = v_d$ with the velocities (2) until one of the following rules applies.

- FII If $N_a/N_d < r_c$ and $p_h < d_1 < a_1$ then increase N_a by one, re-index $a_i \rightarrow a_{i+1}$ for all i and set $a_1 = 0$ (injection of accumulation front).
- FIII If $N_a/N_d > r_c$ and $p_l < a_1 < d_1$ then increase N_d by one, re-index $d_i \rightarrow d_{i+1}$ for all i and set $d_1 = 0$ (injection of depletion front).
- FIV If $a_{i'} = d_{j'}$ for any i', j' then decrease N_a and N_d by one, re-index $a_{i+1} \rightarrow a_i$ for $i \geq i'$ and $d_{j+1} \rightarrow d_j$ for $j \geq j'$ (annihilation of front pair).
- FV If $a_{N_a} > L$ decrease N_a by one (accumulation front hits collector).
- FVI If $d_{N_d} > L$ decrease N_d by one (depletion front hits collector).

Note that the voltage parameter L_h only enters in the initial condition for the front positions (see Eq. (1)).

In the following we will restrict ourselves to the case $r_c < 1$ and $p_l = 0$. Rule FII does not apply as long as $N_a > r_c/(1 - r_c)$ and N_a can then only decrease. Consequently r_c imposes the following limits on the number of fronts:

$$N_d \leq n; \quad N_a \leq n - 1; \quad (3)$$

where n is the largest integer less than $1/(1 - r_c) + 1$. The injection of an accumulation front is immediately followed by the injection of a depletion front (FIII). This detaches a high field domain from the emitter and opens a new one. Furthermore we restrict ourselves to the case where no fronts reach the collector (i.e. $L > nL_h$). This corresponds to the situation in Fig. (1) and we have $N_a = N_d - 1$.

The n-tank model. Under the restrictions given above we may choose the lengths of the high field domains (cf. inset of Fig.1) $x_1 = d_1$ and $x_i = d_i - a_{i-1}$ for $i = 2 \dots N_d$ as new dynamical variables governed by the rules:

TI The lengths evolve according to $\dot{x}_i = -\mu + \lambda \delta_{i1}$ with $\mu = 2/(2N_d - 1)$ and $\lambda = N_d \mu$.

TII If $N_d < n$ and $x_1 > p_h$ then increase N_d by one, re-index $x_i \rightarrow x_{i+1}$ for all i and set $x_1 = 0$.

TIII If $x_{i'} = 0$ then decrease N_d by one, re-index $x_{i+1} \rightarrow x_i$ for all $i \geq i'$.

The voltage constraint (1) is expressed in the new variables by $\sum_k x_k = L_h$.

It is very illustrative to interpret this model in the language of an n -tank switched arrival system (cf. Fig.2). A domain may be viewed as a tank with fluid content x_i . One tank is filled at rate $(N_d - 1)\mu$, while $N_d - 1$ tanks are drained at rate μ , and $n - N_d$ tanks are empty and waiting for filling, because the currently filled tank has not yet reached the minimum filling level $x_{min} = p_h$.

Let us first discuss the limiting case $p_l = p_h = 0$. If a tank is empty at time t_m (i.e. $x_k(t_m) = 0$), the rules TII and TIII apply instantaneously and the system

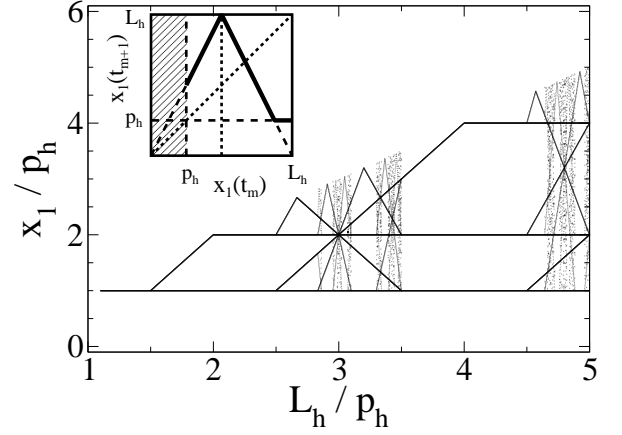


FIG. 4: Bifurcation diagram of x_1 vs. L_h in units of p_h . Inset: Graph of the return map for the $n = 3$ tank model Eq. (5). In the shaded region the map is not defined.

starts to fill this tank ($x_1(t_m^+) = 0$). In this case no tank has to wait for filling. Apart from the re-indexing procedures we obtain a switched arrival system [18]. As shown in [23] the system is chaotic for all $n > 2$ and has a constant invariant probability measure. By sampling the dynamics at the switching times t_m we obtain the *Poincaré map* $P : \vec{x}(t_m) \mapsto \vec{x}(t_{m+1})$:

$$\vec{x}(t_{m+1}) = \vec{x}(t_m^+) + \dot{\vec{x}} \Delta t_m \quad (4)$$

where $\dot{\vec{x}} = (\lambda - \mu, -\mu, \dots, -\mu)$ is a constant vector and $\Delta t_m = t_{m+1} - t_m = \min_{j \neq 1} (x_j(t_m^+)/\mu)$. Generally this is an n dimensional mapping which acts due to the normalization $\sum_i x_i = L_h$ on the $n - 2$ dimensional boundary of a regular n -simplex embedded in \mathbb{R}^n . For $n = 3$ we can reduce this map to a one-dimensional map of the interval $[0, L_h]$ onto itself: From the rules we obtain $x_1(t_m^+) = 0$, $x_2(t_m^+) = x_1(t_m)$, and $x_3(t_m^+) = L_h - x_1(t_m)$. If $x_1(t_m) < L_h/2$, the tank 2 empties after $\Delta t_m = x_1(t_m)/\mu$ and we find $x_1(t_{m+1}) = 2x_1(t_m)$. Otherwise, if $x_1(t_m) > L_h/2$, the tank 3 empties after $\Delta t_m = (L_h - x_1(t_m))/\mu$ and we find $x_1(t_{m+1}) = 2(L_h - x_1(t_m))$. Thus the dynamics is that of the well known *tent map*: $x_1(t_{m+1}) = L_h - 2|x_1(t_m) - L_h/2|$.

Now we consider the case $n = 3$ with a finite minimum filling level $p_h > 0$. Since by TII x_1 must be larger than p_h for switching, the Poincaré map is now only defined on the interval $[p_h, L_h]$. For $x_1 \in [p_h, L_h - p_h/2]$ the map remains unchanged from the tent map discussed before. If the switch to an empty tank occurs at $x_1(t_m) > L_h - p_h/2$, the third tank will be empty before the newly filled tank has reached the minimum filling level p_h . Switching is therefore suppressed until $x_1(t_{m+1}) = p_h$. Thus for $n = 3$ we obtain (cf. inset of Fig.4):

$$x_1(t_{m+1}) = \text{Max} \{ (L_h - 2|x_1(t_m) - L_h/2|), p_h \} \quad (5)$$

The bifurcation structure of this map with respect to L_h is unusual (Fig.4) but has similarities to the flat-topped tent map [24, 25]. Due to the horizontal segments the

map cannot show chaotic behaviour although it undergoes several bifurcation cascades. A trajectory on the tent map segments would explore the attractor of the tent map and will therefore either fall on one of the flat segments or stay at an unstable periodic orbit contained in the remaining part of the tent map. Once arrived at one of the flat segments the trajectory continues on a stable periodic orbit. By analyzing the k -th return map of the modified tent map we find that windows of period k are found inside the intervals $L_h/p_h \in (\frac{2^k-1}{4j-2}, \frac{2^k+1}{4j-2})$ for $j \in I_k \subset \{j \in \mathbb{N} | j \leq 2^{k-2} - 1\}$. Thus higher and higher stable periodic orbits are arising in smaller and smaller intervals.

Discussion. In order to compare the bifurcation diagram of the modified tent map (Fig.4) with the bifurcation diagram of the superlattice model (inset of Fig. 3), we note that the voltage U and the position of front annihilation in the superlattice model correspond to the parameters L_h and $x_1(t_m)$ in the map, respectively. We can therefore identify the periodic windows found in the Poincaré map with the periodic pattern observed in the front model. We note that the bifurcation scenarios agree very well up to voltages of about 1.1V, where a period-3 window occurs (inset of Fig. 3). In particular, the remarkable spider-like structure at 0.9V is found for $L_h/p_h = 3$ in the bifurcation diagram of the map. The reason for this spider is that the contracting flat region is mapped onto the unstable fixed point of the map. Further prominent features in both bifurcation diagrams are the horizontal lines given by the first, and higher iterated images of the minimal filling height. Thus the character

of the bifurcation scenario of complex front dynamics is explained by considering a one-dimensional iterated map with only one free parameter L_h/p_h .

The minimum filling height corresponds to the minimum domain width. For a real superlattice system this quantity will slightly depend on the history of the dynamical evolution. Therefore the slope of the flat segments is not exactly zero but attains a small finite value α . In this case a period- k orbit is unstable if $|2^k \alpha| > 1$. Close to the spider-like points where periodic orbits with large period k occur, we can then find a finite chaotic regime, as observed in our simulations with the microscopic model.

Conclusions. We have introduced a hybrid tank model as a simplified model for front dynamics in nonlinear systems with a global constraint. This simplified model provides an explanation for the complex accumulation and depletion front dynamics in semiconductor superlattices. In this unexpected analogy, the tank filling levels correspond to the widths of the high field domains in the superlattice, while the position of the server determines which high field domain is connected to the emitter. Although this analysis has started from a superlattice model, the presented methods are very general and are expected to work successfully for other systems which provide a global coupling similar to Eq. (1).

Acknowledgments. This work was partially supported by DFG in the framework of Sfb 555 and the Volkswagen Foundation (Grant No. I/76 279 - 280). We thank N. Janson, A. Pikovsky and J. Schlesner for stimulating discussions.

-
- [1] M. C. Cross and P. C. Hohenberg, Rev. Mod. Phys. **65**, 851 (1993).
 - [2] *Chemical Waves and Patterns*, edited by R. Kapral and K. Showalter (Kluwer Academic Publishers, 1995).
 - [3] A. S. Mikhailov, *Foundations of Synergetics Vol. I*, 2 ed. (Springer, Berlin, 1994).
 - [4] J. A. Sherratt, Physica D **117**, 145 (1997).
 - [5] J. Müller and W. van Saarloos, Phys. Rev. E **65**, 061111 (2002).
 - [6] L. Esaki and L. L. Chang, Phys. Rev. Lett. **33**, 495 (1974).
 - [7] J. Kastrup, R. Klann, H. T. Grahm, K. Ploog, L. L. Bonilla, J. Galán, M. Kindelan, M. Moscoso, and R. Merlin, Phys. Rev. B **52**, 13761 (1995).
 - [8] K. Hofbeck, J. Grenzer, E. Schomburg, A. A. Ignatov, K. F. Renk, D. G. Pavel'ev, Y. Koschurinov, B. Melzer, S. Ivanov, S. Schaposchnikov, and P. S. Kop'ev, Phys. Lett. A **218**, 349 (1996).
 - [9] M. Patra, G. Schwarz, and E. Schöll, Phys. Rev. B **57**, 1824 (1998).
 - [10] A. Wacker, Phys. Rep. **357**, 1 (2002).
 - [11] L. L. Bonilla, J. Phys.: Condens. Matter **14**, R341 (2002).
 - [12] O. M. Bulashenko and L. L. Bonilla, Phys. Rev. B **52**, 7849 (1995).
 - [13] K. J. Luo, H. T. Grahm, K. H. Ploog, and L. L. Bonilla, Phys. Rev. Lett. **81**, 1290 (1998).
 - [14] A. Amann, J. Schlesner, A. Wacker, and E. Schöll, Phys. Rev. B **65**, 193313 (2002).
 - [15] E. Schöll, *Nonlinear spatio-temporal dynamics and chaos in semiconductors* (Cambridge University Press, Cambridge, 2001).
 - [16] I. R. Cantalapiedra, M. J. Bergmann, L. L. Bonilla, and S. W. Teitworth, Phys. Rev. E **63**, 056216 (2001).
 - [17] M. D. Graham, U. Middya, and D. Luss, Phys. Rev. E **48**, 2917 (1993).
 - [18] C. Chase, J. Serrano, and P. J. Ramadge, IEEE Trans. Automat. Control **38**, 70 (1993).
 - [19] K. Peters and U. Parlitz, Int. Journ. Bif. Chaos **19**(9), to appear (2003).
 - [20] S. Banerjee and C. Grebogi, Phys. Rev. E **59**, 4052 (1999).
 - [21] A. Carpio, L. L. Bonilla, A. Wacker, and E. Schöll, Phys. Rev. E **61**, 4866 (2000).
 - [22] A. Amann, A. Wacker, L. L. Bonilla, and E. Schöll, Phys. Rev. E **63**, 066207 (2001).
 - [23] T. Schürmann and I. Hoffmann, J. Phys. A **28**, 5033 (1995).
 - [24] L. Glass and W. Zeng, Int. Journ. Bif. Chaos **4**, 1061 (1994).
 - [25] C. Wagner and R. Stoop, J. Stat. Phys. **106**, 97 (2002).